



HAL
open science

A Boundary Element Method Applied to Gas-Liquid Drainage in a Capillary Cavity.

Didier Lasseux, Pierre Fabrie, Michel Quintard

► **To cite this version:**

Didier Lasseux, Pierre Fabrie, Michel Quintard. A Boundary Element Method Applied to Gas-Liquid Drainage in a Capillary Cavity.. C. A. Brebbia; P. W. Partridge. Boundary Elements in Fluid Dynamics, Springer; Computational Mechanics Publications, pp.197-208, 1992, 978-1-85166-780-2. 10.1007/978-94-011-2876-6_15 . hal-03827872v2

HAL Id: hal-03827872

<https://hal.science/hal-03827872v2>

Submitted on 5 Dec 2022

HAL is a multi-disciplinary open access archive for the deposit and dissemination of scientific research documents, whether they are published or not. The documents may come from teaching and research institutions in France or abroad, or from public or private research centers.

L'archive ouverte pluridisciplinaire **HAL**, est destinée au dépôt et à la diffusion de documents scientifiques de niveau recherche, publiés ou non, émanant des établissements d'enseignement et de recherche français ou étrangers, des laboratoires publics ou privés.

A Boundary Element Method Applied to Gas-Liquid Drainage in a Capillary Cavity

D. Lasseux (*), P. Fabrie (*)(**), M. Quintard (*)

(*) *L.E.P.T. - ENSAM (UA CNRS), Esplanade des Arts et Métiers, 33405 Talence Cedex, France*

(**) *UFR de Mathématiques et Informatique*

(CeReMab - UA CNRS), Université Bordeaux I, 33405 Talence Cedex, France

ABSTRACT

The boundary element method is applied to the Stokes problem with a moving boundary in capillary cavities. The numerical method uses a stress/velocity formulation, which is very suitable for the boundary conditions involved. The displacement of the moving surface is calculated explicitly; smoothing and re-gridding insure stability of the overall scheme. The method allows one to simulate directly the behavior of very thin dynamic films left behind a receding meniscus. The numerical results are compared with both experimental observations and calculations based on a simplified theoretical analysis.

INTRODUCTION

Drainage processes in porous media are of great practical importance in petroleum engineering, a typical problem being gas-oil drainage in the presence of water. Micromodel studies (Chatzis et al., 1988¹) suggest that these flows are largely influenced by the existence of dynamic films left behind receding menisci. These mechanisms are highly sensitive to pore geometry; however, direct numerical simulations, simplified theoretical results, and experimental studies for simple capillary geometries can help understand the dynamics of such flows.

Simplified solutions, based on lubrication-type approximations, are available for flow in tubes (Bretherton²) or in Hele Shaw cells (Park et Homsy³). In these configurations, it is possible to derive a simple relationship between the film thickness, e , and the capillary number, Ca , in the following form

$$e/b = 1.337 Ca^{2/3} \quad (1)$$

where b is half the distance between the two plates in the Hele Shaw case. In addition to the lubrication-type approximation, this result is based on several simplifications such as: (i) the film thickness is supposed to be constant in a region far from the meniscus, (ii) the Bond number, Bd , is assumed to have negligible effect on the flow. Furthermore, the correlation given by Equation (1) is not valid for large capillary numbers for obvious reasons. Thus, it is

very attractive to obtain a full solution of the two-phase flow problem to extend the range of validity of the above correlation.

For more complex geometries, dimensional analysis suggests that such a correlation exists. However, such numerical boundary problems, the boundary element method is very attractive. It can be tested on the simple geometries mentioned above. The Bretherton problem has been studied numerically by Lu⁴. In this paper, we present a numerical solution of the Hele Shaw case. We consider the drainage of a wetting phase (liquid) by a gas phase, the flow taking place between two plates as it is illustrated in Figure 1.

NUMERICAL METHOD

The two-phase flow free boundary problem under consideration is solved numerically using a boundary element technique. This method has proved to be suitable and accurate in many cases of free surface flow as reported in Wrobel and Brebbia⁵.

The liquid domain Ω and its boundary $\partial\Omega=S_1\cup S_2\cup S_3$ are illustrated in Figure 1. The liquid phase is limited on each side by two vertical, impermeable, rigid boundaries S_2 . The distance between the two vertical planes is equal to $2b$. The lower boundary corresponds to a fictitious horizontal plane S_3 in the liquid phase. The upper gas phase is separated from the liquid by the free surface S_1 .

The velocity field on S_3 is a Poiseuille flow at a constant flow rate. We assume that the flow pattern in Ω is purely two-dimensional in the plane ($\mathbf{e}_x, \mathbf{e}_z$) represented in Figure 1. Furthermore, we assume that: (i) the viscosity and the density of the gas phase are negligible compared to the viscosity and the density of the liquid phase; (ii) the drainage velocity is small enough for the Stokes approximation to be valid in the liquid phase.

As a consequence, the boundary value problem can be written as follows

$$\nabla \cdot \mathbf{S} = \mathbf{0} \quad (2)$$

$$\nabla \cdot \mathbf{v} = 0 \quad (3)$$

in the liquid phase, where \mathbf{S} is the stress tensor, and \mathbf{v} the dimensionless velocity.

The appropriate boundary conditions are

$$\text{(B.C. 1)} \quad \mathbf{v}|_{S_2} = \mathbf{0} \quad (4)$$

$$\text{(B.C. 2)} \quad \mathbf{v}|_{S_3} = (h^2 - 1)\mathbf{e}_z \quad (5)$$

$$\text{(B.C. 3)} \quad \mathbf{n} \cdot \mathbf{S} = \left[\frac{1/R - Bd z}{Ca_0} \right] \mathbf{n} \quad (6)$$

Because of the assumptions we have made, the pressure in the gas phase is assumed to be constant, equal to P_0 .

In Equation (2) \mathbf{S} is the dimensionless stress tensor defined by

$$\mathbf{S} = -p \mathbf{I} + \nabla \mathbf{v} + {}^t \nabla \mathbf{v} \quad (7)$$

in which p is the dimensionless pressure in the liquid phase. The dimensionless velocity is defined from the dimensional corresponding variable, denoted with superscript *, by

$$\mathbf{v} = \mathbf{v}^*/V_0 \quad (8)$$

where V_0 is the reference velocity on the symmetry axis on S_3 . Similarly the dimensionless pressure is defined by

$$p = \frac{p^* - P_0 + \rho g b z}{\mu V_0} \quad (9)$$

where ρ , μ , and g represent the density, the viscosity of the liquid phase and the gravitational acceleration respectively; h and z are the coordinates made dimensionless by b .

In Equation (6), R is the dimensionless radius of curvature at the point of S_1 located at position z ; Bd and Ca_0 are respectively the Bond number and the capillary number defined by

$$Bd = \rho g b^2/\gamma \quad (10)$$

$$Ca_0 = \mu V_0/\gamma \quad (11)$$

in which γ is the interfacial tension.

While the liquid phase flows, the free surface S_1 , of equation $\Phi(h,z,t) = 0$, evolves following the classical kinematic condition

$$\frac{D\Phi}{Dt} = \frac{\partial \Phi}{\partial t} + \mathbf{v} \cdot \nabla \Phi = 0 \quad (12)$$

From Equations (2) and (3), one forms the boundary integral equation of the problem (see DaCosta Sequeira⁶ and Lasseux⁷ for details) which can be written as

$$\int_{\partial\Omega} \mathbf{n}_k \cdot [\mathbf{S}(\mathbf{u}_k(\mathbf{x} - \mathbf{y}), t_k(\mathbf{x} - \mathbf{y})) \cdot \mathbf{v}(\mathbf{x}) - \mathbf{S}(\mathbf{v}(\mathbf{x}), p(\mathbf{x})) \cdot \mathbf{u}_k(\mathbf{x} - \mathbf{y})] d\gamma = 0 \quad (13)$$

$k = 1, 2$

for any points \mathbf{x} and \mathbf{y} on $\partial\Omega$. In this formula, $(\mathbf{u}_1, \mathbf{u}_2)$ and \mathbf{t} are the fundamental solution of the elementary two-dimensional Stokes problem

$$-\nabla \cdot [(\nabla \mathbf{u}_k(\mathbf{x} - \mathbf{y}) + {}^t \nabla \mathbf{u}_k(\mathbf{x} - \mathbf{y})) - t_k(\mathbf{x} - \mathbf{y}) \mathbf{I}] = \delta(\mathbf{x} - \mathbf{y}) \mathbf{e}_k \quad k=1, 2 \quad (14)$$

where $\delta(\mathbf{x} - \mathbf{y})$ is the Dirac distribution at point \mathbf{y} .

This fundamental solution can be found for example in DaCosta Sequeira⁶ or in Ladyzhenskaya⁸ and is given by

$$\mathbf{u}_{t_k}(\mathbf{x} - \mathbf{y}) = \frac{1}{4\pi} \left[-\delta_{t_k} \ln r + \frac{(y_t - x_t)(y_k - x_k)}{r^2} \right] \quad (15)$$

$$t_k = \frac{1}{2\pi} \frac{\partial \ln r}{\partial x_k} \quad (16)$$

with

$$r = |\mathbf{x} - \mathbf{y}| \quad (17)$$

According to the boundary conditions for the problem considered here, equation (13) can be re-written in a more convenient form as

$$\int_{S_2 \cup S_3} \mathbf{n} \cdot [\mathbf{S}(\mathbf{v}(\mathbf{x}), p(\mathbf{x})) \cdot \mathbf{u}_k(\mathbf{x} - \mathbf{y})] d\gamma - \int_{S_1} \mathbf{n} \cdot [\mathbf{S}(\mathbf{u}_k(\mathbf{x} - \mathbf{y}), t_k(\mathbf{x} - \mathbf{y})) \cdot \mathbf{v}(\mathbf{x})] d\gamma =$$

$$\int_{S_2 \cup S_3} \mathbf{n} \cdot [\mathbf{S}(\mathbf{u}_k(\mathbf{x} - \mathbf{y}), t_k(\mathbf{x} - \mathbf{y})) \cdot \mathbf{v}(\mathbf{x})] d\gamma - \int_{S_1} \mathbf{n} \cdot [\mathbf{S}(\mathbf{v}(\mathbf{x}), p(\mathbf{x})) \cdot \mathbf{u}_k(\mathbf{x} - \mathbf{y})] d\gamma$$

$$k = 1, 2 \quad (18)$$

At this point, it is seen that the velocity/normal stress formulation is very suitable for the problem under consideration since the boundary conditions appear directly in the above equation. This last equation allows to compute the normal stress $\mathbf{n} \cdot \mathbf{S}$ on $S_2 \cup S_3$, and \mathbf{v} on the *moving boundary* S_1 .

Discretization:

The continuous problem (Equations (2) to (6) and (12)) is now discretized in order to produce a linear system and give the unknown values on $\partial\Omega$ (Huyakorn and Pinder⁹). Our computation has been performed using a *constant boundary elements* method which consists in dividing the boundary $\partial\Omega$ into m straight line segments Γ . On each segment, $\mathbf{n} \cdot \mathbf{S}$ and \mathbf{v} are assumed to have a constant value, equal to the value at the central node.

The choice for constant boundary elements is mainly justified by the fact that this method gives an accurate approximation of the solution either on the boundary or for points inside the domain far enough from the boundary. This has also been pointed out in other works concerning free surface flows of viscous newtonian fluids (Bush¹⁰). In addition, the numerical scheme for constant boundary elements is fast and simple to implement, making this method a very attractive one (Bush¹⁰, Lu⁴, Sugino and Tosaka¹¹).

The first step is to discretize the boundary integral given by Equation (18). This is done by writing

$$\sum_{j=m_1+1}^{m_1+m_2+m_3} \left[(\mathbf{n}_j \cdot \mathbf{S}(\mathbf{v}_j, p_j)) \cdot \int_{\Gamma_j} \mathbf{u}_k(\mathbf{x}_j - \mathbf{y}_i) d\gamma_j \right] -$$

$$\sum_{j=1}^{m_1} \left[\int_{\Gamma_j} \mathbf{n}_j \cdot \mathbf{S}(\mathbf{u}_k(\mathbf{x}_j - \mathbf{y}_i), t_k(\mathbf{x}_j - \mathbf{y}_i)) d\gamma_j \right] \cdot \mathbf{v}_j =$$

$$\sum_{j=m_1+1}^{m_1+m_2+m_3} \left[\int_{\Gamma_j} \mathbf{n}_j \cdot \mathbf{S}(\mathbf{u}_k(\mathbf{x}_j - \mathbf{y}_i), t_k(\mathbf{x}_j - \mathbf{y}_i)) d\gamma_j \right] \cdot \mathbf{v}_j -$$

$$\sum_{j=1}^{m_1} \left[(\mathbf{n}_j \cdot \mathbf{S}(\mathbf{v}_j, p_j)) \cdot \int_{\Gamma_j} \mathbf{u}_k(\mathbf{x}_j - \mathbf{y}_i) d\gamma_j \right]$$

for $k=1,2$ and $i=1, m_1+m_2+m_3$ (19)

In this relation, χ_j means that χ is taken at node j (or on the j^{th} element); \mathbf{x}_j and \mathbf{y}_i denote positions of nodes j and i on $\partial\Omega$; m_l is the number of nodes (or elements) on S_l , $l=1,3$. Node numbering is such that the node number increases while $\partial\Omega$ is described clockwise and node number one is the first node on S_1 which has a positive h coordinate. We will denote m as the total number of nodes ($m=m_1+m_2+m_3$).

The next step consists in discretizing the boundary conditions given by Equations (4) through (6). According to the method used here, this can be done by writing

$$(B.C. 4) \quad \mathbf{v}_j = \mathbf{v}|_{\Gamma_j} = \mathbf{0} \quad j=m_1+1, m_1+m_2 \quad (20)$$

$$(B.C. 5) \quad \mathbf{v}_j = \mathbf{v}|_{\Gamma_j} = (h_j^2 - 1)\mathbf{e}_z \quad j=m_1+m_2+1, m_1+m_2+m_3 \quad (21)$$

$$(B.C. 6) \quad (\mathbf{n} \cdot \mathbf{S})_j = \left[\frac{1/R_j - Bd z_i}{Ca_0} \right] \cdot \mathbf{n}_j \quad j=1, m_1 \quad (22)$$

where R_j and \mathbf{n}_j are the radius of curvature of S_1 at node j and the unit outward normal vector of element j respectively.

At this point, one clearly sees that the right hand side of Equation (19) is completely known. In addition, the symmetry of the problem gives a solution symmetric with respect to the z -axis. Therefore the number of unknowns is reduced accordingly.

From Equations (15), (16) and (19), it is clear that the fundamental solution of the elementary two dimensional Stokes problem has singularities at each interpolation node. However, because of the constant boundary elements method retained here, each integral in Equation (19) can be explicitly calculated (see Lasseux⁷), therefore avoiding the use of approximations with quadrature formulae such as those used in Sato et al.¹².

The last discretization step consists of finding a suitable discretized form of Equation (12). Points on the free boundary are moved according to

$$\mathbf{z}_j^{n+1} = \mathbf{z}_j^n + \delta t \mathbf{v}_j^n \cdot \mathbf{e}_z \quad (23)$$

$$h_j^{n+1} = h_j^n + \delta t \mathbf{v}_j^n \cdot \mathbf{e}_h \quad (24)$$

where δt represents the time step, and superscripts n and $n+1$ denote variables at time steps n and $n+1$ respectively. Equations (23) and (24) are the approximate form of Equation (12) using an explicit Euler method. This approximation has also been employed successfully for updating the free boundary in Sugino and Tosaka¹¹ and Sato et al.¹².

In this work, the relations (23) and (24) have been used with the empirical stability condition

$$\delta t < Ca_0/10 \quad (25)$$

which expresses the fact that the time step is inversely proportional to the normal stress on S_1 (see for example (B.C. 3) in Equation (6)).

Even under the constraint expressed by Equation (25), the updating process described by Equations (23) and (24) generates instabilities which can be observed after only few time steps. This fact has also been noted by Sugino and Tosaka¹¹. The reason for this lies in the fact that the element size on S_1 is altered by the updating process. This is due to the velocity gradient along S_1 which causes elements near the symmetry axis to become larger while elements near S_2 become smaller. To remedy this problem, a smoothing and relocation technique has been used. At each time step, the free boundary S_1 is smoothed with local cubic spline functions. These piecewise functions allow one to relocate and eventually add nodes on S_1 in order to keep an approximately constant element size during the whole computation. In addition, as the z coordinate of the lower point on S_1 decreases, it is necessary to increase the vertical size of the domain, i.e., increase the number of nodes m_2 on S_2 .

Numerical experiments showed that the above mentioned instabilities are dramatically enhanced when capillary effects are dominant, and this increases the stiffness of the problem while an accurate evaluation of the radius of curvature R of S_1 (see Equation (22)) is required. As the spline functions are only piecewise functions, the evaluation of this last quantity by direct derivation has proved to be unsatisfactory. Hence, the value of R_j is approximated by averaging the distances along the normal line from the j^{th} node to the intersections of the normal lines from the adjacent nodes.

The free boundary is set initially to be the discretized solution of the gravity/capillary two-phase equilibrium. This solution is detailed in Lasseux⁷. Finally, the algorithm is summarized below as

- 1) The radius of curvature on S_1 is evaluated as described above.
- 2) Discretized boundary conditions are computed at each node.
- 3) Integrals in Equation (19) are calculated and the linear system is formed.
- 4) The linear system is then solved, providing \mathbf{v}_j on S_1 and $(\mathbf{n} \cdot \mathbf{S})_j$ on S_2 and S_3 . The system is solved by using a QR factorizing method. This method has been chosen on the basis of stability criteria, knowing that the system matrix, which is fully populated and non symmetric, is more ill

conditioned as the discretization is refined. An alternative algorithm for solving this type of system can be found in Cai et al.¹³.

- 5) The free boundary is updated according to Equations (23) (24) and (25).
- 6) The boundary S_1 is smoothed. Boundaries S_1 and S_2 are re-gridded, keeping the initial element size and vertical extent.

Calculations continue until a significant volume of fluid is displaced. At each time step, precision is checked via the fluid volume balance, which is better than 1% for all our simulations.

Results

Our simulations have been performed for two values of the Bond number ($Bd = 0$ and $Bd = 1.03$) and different values of the capillary number. As the total calculation time becomes prohibitive when the capillary number is small (see Equation (25)), our numerical experiments are performed for capillary numbers greater than $2 \cdot 10^{-3}$. In addition, our numerical experiments presented here are limited to the case of perfectly wetting liquid.

In Figure 2 are shown the right hand side shapes of the symmetrical free surface for various times and the two Bond numbers. This figure clearly shows the wetting film, of approximately constant thickness, on the immobile boundary S_2 . Furthermore, the important effect of the Bond number is unambiguously outlined as a much thicker film is obtained when gravity forces are set equal to zero. This is confirmed on Figure 3 where our numerical results, in terms of film thickness, are represented as a function of the capillary number and the Bond number. These results suggest that a consistent power law relationship between the film thickness, e , (computed at $z = (z_{m1} - z_1)/2$) and the capillary number Ca (calculated from the mean velocity V of the first node on S_1 during the overall computation) can be found. As shown in this figure, this kind of relationship is valid for capillary numbers smaller than 0.1. A power law fitted to these numerical results, in this range of capillary numbers, gives

$$e/b = 0.71 Ca^{2/3} \quad ; \quad Bd = 1.03 \quad (26)$$

$$e/b = 1.17 Ca^{2/3} \quad ; \quad Bd = 0 \quad (27)$$

These results are compared with our theoretical and experimental ones in the following. It should be noticed however that the last equation is in good agreement with the analytical result given by Park and Homsy³. In addition, for large values of the capillary number ($Ca > 0.1$), our calculations indicate that the film thickness reaches an asymptotical value of 0.35. This value has also been obtained in several experimental, theoretical and numerical works in similar cases (Reinelt and Saffman¹⁴, Schwartz et al.¹⁵, and Lu⁴).

THEORETICAL RESULTS

The theoretical approach we developed for an approximate analysis of the free boundary problem is summarized below (see Park and Homsy³ for details). Our calculations are performed in a coordinate system fixed relative

to the lower point of the free surface moving downward at a constant velocity V . The free boundary, which is assumed to be symmetric with respect to e_z , is divided into three regions: (1) the region far upstream from the meniscus, called the film developed region, in which capillary forces are small and where the film thickness is assumed to be stationary and equal to e_0 ; (2) the transition region where all the forces involved in the physical process are of the same order of magnitude, a priori; the film thickness is denoted e in this region; (3) the meniscus region, which is assumed to be identical to the meniscus at equilibrium under capillary and gravity forces in the same cavity (this requires that the capillary number is small).

In region (1) and (2), the lubrication approximation is retained. After the flow rate balance condition is fulfilled between these two regions, and assuming that

$$Ca = \frac{\mu V}{\gamma} \ll 1 \quad (28)$$

one can write the approximate differential equation governing the free surface shape away from the meniscus in a dimensionless form as

$$X_{\epsilon\epsilon\epsilon} = \frac{1-X}{X^3} \quad (29)$$

with

$$X = e / e_0 \quad (30)$$

$$\epsilon = (3 Ca)^{1/3} z/e_0 \quad (31)$$

The associated boundary conditions are

$$(B.C. 7) \quad X \rightarrow 1 \quad \text{as} \quad \epsilon \rightarrow +\infty \quad (32)$$

$$(B.C. 8) \quad X_\epsilon \rightarrow 0 \quad \text{as} \quad \epsilon \rightarrow +\infty \quad (33)$$

$$(B.C. 9) \quad X_{\epsilon\epsilon} \rightarrow 0 \quad \text{as} \quad \epsilon \rightarrow +\infty \quad (34)$$

The boundary condition (B.C. 8) indicates that the liquid perfectly wets the solid, which is the restriction of our study.

While the flow pattern is complicated in the meniscus region (its description is beyond the scope of this paper), a satisfactory matching condition between the transition region and the meniscus region is given by the required continuity of the curvature (i.e. the capillary pressure) instead of the flow rate balance. In fact, when the liquid perfectly wets the solid, this matching condition is equivalent to the continuity of the second derivative of X .

Hence, it is necessary to investigate the second derivative behavior of the profile in the transition region as the meniscus region is approached, knowing that e is expected to be large compared to e_0 when approaching the meniscus. This requires integrating Equation (29) to determine the limit value of $X_{\epsilon\epsilon}$ as X tends to infinity. After returning to the dimensional form, we obtain (with the notation $\Phi = b - e$)

$$|e_{zz}| = |\Phi_{zz}| = 1.338 Ca^{2/3} / e_0 \quad (35)$$

while approaching the meniscus region. In addition, from the study of the meniscus at equilibrium ($h = \Phi(z)$), we get the following equation

$$|\Phi_{zz}| = Bd \lambda_2 / b \quad (36)$$

at a point $z=b \lambda_2$ corresponding to the contact point, $z = 0$ corresponding to the flat interface level outside the plates. Matching $|\Phi_{zz}|$ between Equations (35) and (36) yields

$$e_0 / b = \frac{1.338 Ca^{2/3}}{Bd \lambda_2} \quad (37)$$

It can be shown (Lasseux⁷) that this important result is valid for any Bond number. Equation (37) gives Equation (1) when $Bd=0$, and when $Bd=1.03$ we have

$$e_0 / b = 0.81 Ca^{2/3} \quad (38)$$

As can be seen from Equations (26), (27), (1) and (38), numerical results for the film thickness are in good agreement with these analytical predictions. This comparison confirms the consistency of a power law relationship between the dimensionless film thickness and the capillary number ($Ca < 0.1$) and the important effect of the Bond number on the physical process.

Our own experimental results are now presented and compared to both of the above mentioned approaches.

COMPARISON WITH EXPERIMENTAL RESULTS

Several drainage experiments of different silicone oils by air have been performed for capillary numbers ranging from $5 \cdot 10^{-5}$ to $2 \cdot 10^{-2}$ using a vertical Hele Shaw cell (Lasseux and Quintard¹⁶). These experiments were such that: (i) the cell walls were perfectly wetted by the oils; (ii) the Bond number was constant equal to 1.03 for all the experiments; (iii) the temperature was constant, equal to 20 °C.

The Hele Shaw cell was first saturated with oil to the height Z_0 and then drained at a constant flow rate using a syringe pump until the meniscus reached the position Z_1 ($|Z_0 - Z_1| \approx 150 b$). This stage corresponds to the physical problem studied in this paper. In order to estimate the film thickness, the experiments were subsequently conducted as follows. The bulk drainage was stopped and fluids inside the cell were isolated. Then, the film remaining on the walls drained under gravity and produced a free surface rise until final equilibrium, for which the interface reached a position labelled Z_f . All the positions referred above are those of the lower point of the meniscus on the cell symmetry axis and were detected by photographs. The capillary number was evaluated using the mean velocity of the lower point of the interface, calculated from the positions of this point during the bulk drainage period.

From a volume balance equation, assuming that the film thickness, e , is constant during the bulk drainage, and neglecting the adsorbed film, it can be shown that

$$e / b = \frac{Z_f - Z_1}{Z_0 - Z_1} \quad (39)$$

In Figure 4 are reported our experimental dimensionless film thickness results versus the capillary number, together with the numerical and analytical predictions. The comparison shows a rather good agreement since the following power law

$$e / b = (0.97 \pm 0.14) Ca^{(0.67 \pm 0.02)} \quad (40)$$

has been fitted on our experimental data.

CONCLUSION

A boundary element method has been successfully developed to describe the Stokes free boundary value flow within two plane parallel plates (Hele Shaw cell). Our numerical code allows to determine the film thickness behind the receding interface during the constant flow rate drainage of a wetting liquid by a gas with a good accuracy. The numerical results are in good agreement with both extended analytical predictions of the film thickness for any value of the Bond number and with experimental data when the capillary number is smaller than 0.1. In this range of capillary number, the consistency of a power law relationship between the film thickness and the capillary number is unambiguously outlined. Furthermore, the important effect of the Bond number on the physical process is confirmed. For large capillary numbers ($Ca > 1$) and any value of the Bond number, a limit film thickness is obtained. This limit value corresponds to that reported in the literature.

Acknowledgement: This work was supported by Institut Français du Pétrole.

REFERENCES

1. Chatzis, I., Kantzas, A. and Dullien, F.A.L. On the investigation of gravity assisted inert gas injection using micromodels, long Berea cores and computer assisted tomography, SPE paper 18284, *63rd SPE Annual Technical Conf. and Exhibition*, Houston, 1988.
2. Bretherton, F.P. The motion of long bubbles in tubes, *J. Fluid Mech.* 10, 166-188, 1961.
3. Park, C.W. and Homsy, G.M. Two-phase displacement in Hele Shaw cells: Theory, *J. Fluid Mech.* 139, 291-308, 1984.
4. Lu, W.Q. 'Boundary Element Analysis of Free Surface Problems of Axisymmetric Taylor Bubbles', *Boundary Elements XII*, Edited by M. Tanaka, C.A. Brebbia and T. Honna, Springer-Verlag, New York. Pro. 12th Int. Conf. on Boundary Elements in Engineering, Sapporo, September 1990.

5. Wrobel, L.C. and Brebbia, C.A. (Ed.) 'Fluid Flow', Section 4, *Free Surface Flow*, Pro. 1st Int. Conf. on Computational Modelling of Free and Moving Boundary Problems, Southampton, CML Publications, Southampton, Boston, 1991.
6. DaCosta Sequeira, A. Couplage entre la méthode des éléments finis et la méthode des équations intégrales: application au problème de Stokes extérieur dans le plan, Thèse Doc. Université de Paris VI, 1981.
7. Lasseux, D. Caractérisation expérimentale, analytique et numérique d'un film dynamique lors du drainage d'un capillaire, Thèse Doc. Université de Bordeaux I.
8. Ladyzhenskaya, O.A. *The Mathematical Theory of Viscous Incompressible Flow*, Gordon & Breach, New York, 1969.
9. Huyakorn, P.S. and Pinder, G.F. *Computational Methods in Subsurface Flow*, Academic Press, 1983.
10. Bush, M.B. 'Stratified Flows of Newtonian Viscous Liquids', Boundary Elements XII, Edited by M. Tanaka, C.A. Brebbia and T. Honna, Springer-Verlag, New York. Pro. 12th Int. Conf. on Boundary Elements in Engineering, Sapporo, September 1990.
11. Sugino, R. and Tosaka, N. 'Boundary Element Analysis of Unsteady Nonlinear Surface Wave on Water', Boundary Elements XII, Edited by M. Tanaka, C.A. Brebbia and T. Honna, Springer-Verlag, New York. Pro. 12th Int. Conf. on Boundary Elements in Engineering, Sapporo, September 1990.
12. Sato, K., Tomita, Y., and Shima, A. 'Numerical Analysis of the Behavior of a Cavitation Bubble near a Vibrating Rigid Wall by the Boundary Integral Method', Boundary Elements XII, Edited by M. Tanaka, C.A. Brebbia and T. Honna, Springer-Verlag, New York. Pro. 12th Int. Conf. on Boundary Elements in Engineering, Sapporo, September 1990.
13. Cai, R.Y., Zeng, Z.J., and Chen F. 'A Partitioning Solution of Non-Symmetrical Fully Populated Matrix System in the Boundary Element Method and its Subroutines', Boundary Elements XII, Edited by M. Tanaka, C.A. Brebbia and T. Honna, Springer-Verlag, New York. Pro. 12th Int. Conf. on Boundary Elements in Engineering, Sapporo, September 1990.
14. Reinelt, D.A., and Saffman, P.G. The penetration of a finger into a viscous fluid in a channel and tube, *SIAM J. Sci. Stat. Comput.* 6 (3), 542-561, 1985.
15. Schwartz, L.W., Princen, H.M., and Kiss, A.D. On the motion of bubbles in capillary tubes, *J. Fluid Mech.* 172, 259-275, 1986.
16. Lasseux, D., and Quintard, M. Epaisseur d'un film dynamique derrière un ménisque récessif, to be published in *C. R. Acad. Sc. Paris, Série II*, 1991.

Boundary Elements in Fluid Dynamics

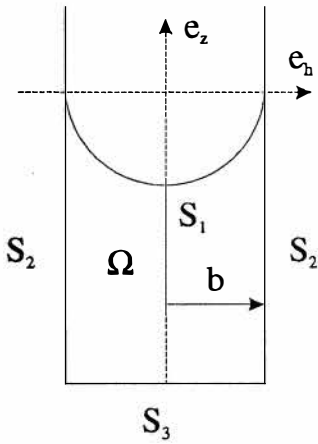


Figure 1. Geometry.

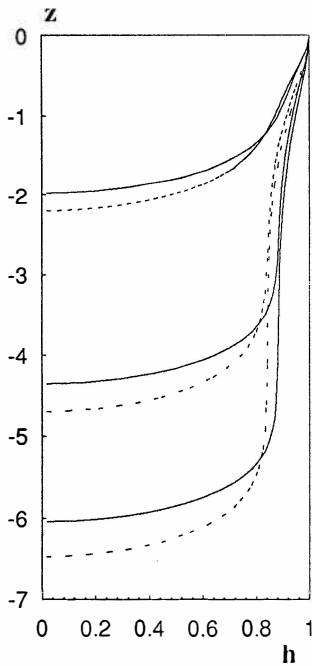


Figure 2. Position of the interface at $t_1=1.44$, $t_2=4.48$, $t_3=7$ for $Ca_0=1$. The solid line corresponds to $Bd=1.03$, the discontinuous line corresponds to $Bd=0$.

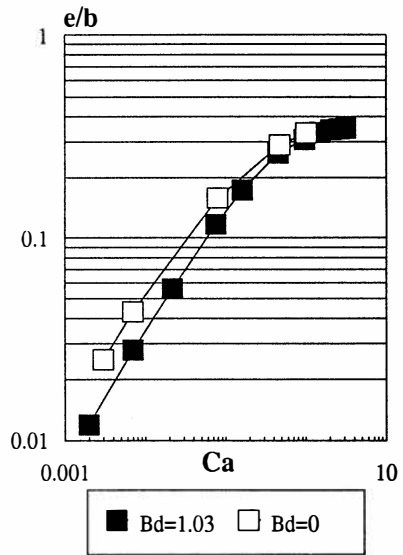


Figure 3. Numerical results.

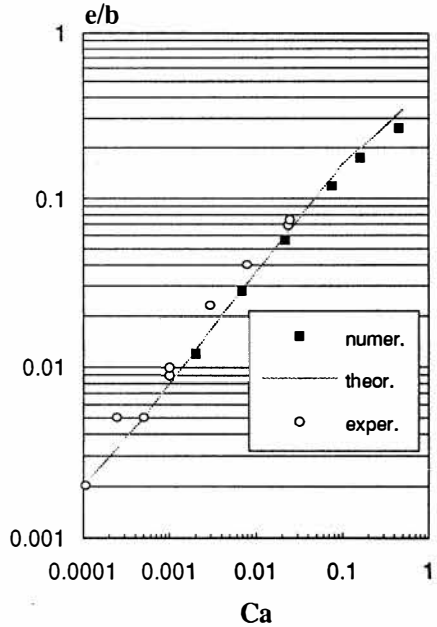


Figure 4. Comparison of the results obtained for $Bd=1.03$.